



COMPARISON OF DIFFERENT TECHNIQUES FOR ROTATING BEAMFORMING AT THE UNIVERSITY OF SÃO PAULO FAN RIG TEST FACILITY

Luciano C. Caldas¹, Paulo C. Greco², Carlos C. Pagani³ and Luiz A. Baccalá⁴
^{1,4} Poli-USP
São Paulo, 05508-900, Brazil
^{2,3} EESC-USP
São Carlos, 13566-590, Brazil

Abstract

Two different techniques for virtual rotating microphones are compared using (a) time domain linear interpolation and (b) frequency domain motion compensation for in-duct beamforming to locate fan noise rotating sources in the newly constructed fan rig test facility at the University of São Paulo - Brazil. The rig has a 16-bladed fan rotor and 14-vaned stator, speeds up to 4250 RPM and 0.1 Mach number mean flow speed. Acoustic data is acquired from a wall-mounted 77-microphone circular array. The in-house developed beamforming software is able to generate both the acoustic noise map and the modal breakdown analysis. Conventional rotating beamforming with modal steering vectors and Clean-SC deconvolution are examined and contrasted for both techniques, in addition to the power spectral density for each technique. Different results obtained for both are quite visible. One led to better results in terms of higher spatial resolution whereas the other to more smeared sources in the noise map. Blade tip and root noise was clearly visible.

1 INTRODUCTION

The aim of this paper is to compare two different techniques for virtual rotating microphones (VRM) commonly used for rotating beamforming imaging. The techniques are compared using experimental data provided by the newly constructed long-duct low-speed fan rig test facility at the São Carlos Engineering School at the University of São Paulo (USP) - Brazil [2].

The rig has 0.6 m diameter and it is about 12 m long from the bell-mouth to the anechoic termination, as depicted in Fig. 1. Its basic configuration comprises a 0.5 m diameter duct fan stage equipped with a 16-bladed rotor and a 14-vaned stator, Fig. 2b. The rotor is powered by an 100 hp electrical motor fixed by 3 struts allowing experiments up to 4250 RPM and 0.1 Mach

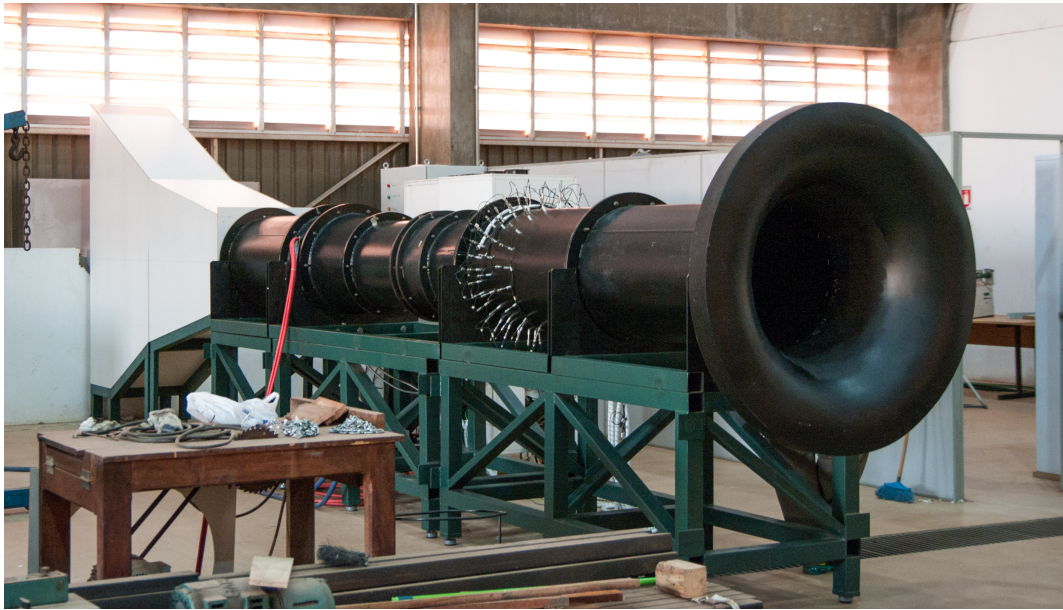


Figure 1: Overview of the USP fan rig - Brazil. The bell-mouth inlet is seen followed by the 77-mics array (upstream of the rotor) and in the end the anechoic termination (white part).



(a) The 3-rings 77-microphones array

(b) Details of the 0.5 m diameter 16-bladed fan.

Figure 2: Closer look at the acoustic array mount and fan rotor.

number based on the mean axial flow speed. Its long duct configuration is similar to that of the DLR low speed fan rig [4] but different from other rigs that operate inside anechoic chambers [6, 12].

An array comprising 77-microphones as portrayed in Fig. 2a was designed. It consists of three rings 0.10 and 0.17 m apart. The ring closer to the fan lies 0.86 m from it and comprises

33 uniformly distributed microphones, whereas the other rings have 23 and 21.

The acoustic data acquisition system comprises duct-wall flush-mounted microphones (GRAS 40PH-S2 ϕ 7 mm, bandwidth of 20-20 kHz and 50 mV/Pa average sensitivity) operated via a PXI National Instruments system composed of 5 PXI-4496 boards. Motor angular position is also acquired simultaneously.

This paper is organized as follows. Section 2 is a brief review of rotating beamforming formulation in terms of steering vector; Section 3 provides details of both array signal processing methods for virtual rotating microphones to be compared; Section 4 gives comparative results in terms of power spectral density (PSD), conventional beamforming maps and Clean-SC deconvolution maps. The paper ends with a brief discussion.

2 ROTATING BEAMFORMING REVIEW

Rotating beamforming has a quite similar formulation as static beamforming in terms of steering vector. For both rotating and static conventional beamforming we estimate the spatial pressure density b_s at a mesh point ξ_s by using

$$b_s = \vec{w}_s C \vec{w}_s^H \quad (1)$$

where $C^{N \times N}$ is the cross-spectral Hermitian matrix at frequency ω between the N microphone pairs and \vec{w}_s is the normalized steering vector at frequency ω and evaluated at the mesh point ξ_s to the microphone positions \vec{x}_i , i.e.

$$\vec{w}_s = \frac{\vec{g}_s}{\|\vec{g}_s\|} \quad (2)$$

where

$$\vec{g}_s := \vec{g}(\vec{x}, \vec{x}_s, \omega) = [g_1(\vec{x}_1, \vec{x}_s, \omega), g_2(\vec{x}_2, \vec{x}_s, \omega), \dots, g_N(\vec{x}_N, \vec{x}_s, \omega)]^T \quad (3)$$

and each element $g_i(\vec{x}_i, \vec{x}_s, \omega)$ computes the transfer function of the travel path from the microphone \vec{x}_i to the mesh point source ξ_s at a given frequency ω . The steering vector used here is the same as the one suggested by Dougherty *et al.* [3] for a solution of the wave equation within a duct

$$g(\vec{r}_i, \vec{r}_s, \omega) = \sum_{m,n} \varphi^*(\vec{r}_s) \varphi(\vec{r}_i) \quad (4)$$

and the solution for a circular section with radius a is given by

$$g(\vec{r}_i, \vec{r}_s, \omega) = \sum_{m=-m^-}^{m^+} \sum_{n=0}^{n^+} \frac{J_m(k_{m,n} r_i) J_m(k_{m,n} r_s)}{N_{m,n}^2} e^{jm(\theta_i - \theta_s)} e^{-jk_z^-(z_i - z_s)} \quad (5)$$

where $J_m(x)$ is the Bessel function of first kind, $\vec{r} = (r, \theta, z)$ is in cylindrical coordinates, subscripts i and s refer to microphone and mesh point indexes, respectively. k_z^- is the axial wave number. Values of $k_{m,n}$ are computed in a way that $J'_m(k_{m,n} a) = 0$, i.e., the product $k_{m,n} a$ is the n^{th} stationary point of order m of the Bessel function $J_m(x)$. A table of these stationary values is reported in [1]. So, for each stationary value $k_{m,n} a$ corresponding to a combination of modes

(m, n) we have an associated axial wave number k_z^- .

The formulation presented above works for stationary beamforming within a duct. In the rotating reference frame, as detailed in [3] and [7], a small change must be performed in the axial wave number, in the manner that

$$k_z^- = \frac{-k'_0 M - \sqrt{k'^0_0{}^2 - (1 - M^2)k_{m,n}^2}}{1 - M^2} \quad (6)$$

where M is the Mach number. k'_0 is the wave number in the rotating frame, given by

$$k'_0 = k_0 - \frac{m\Omega}{c} \quad (7)$$

for each spinning mode m where k_0 is the free wave number, i.e., $k_0 = \omega/c$. Ω is the angular speed of the fan.

Eq. 7 can be seen as a shift-frequency in the rotating frame. Another way to see that is

$$\omega' = \omega - m\Omega \quad (8)$$

which is exactly the frequency shift caused by the modes due to the shaft spinning speed, i.e., in the rotating frame the observed frequency ω' is equivalent to the ω observed.

The terms $m^- \leq m \leq m^+$ and $0 \leq n \leq n^+$ are determined according to Eq. 9, i.e., in the range of cut-on modes. One mode (m, n) is called a *cut-on* mode when the term within the square root of Eq. 6 is positive

$$k'^0_0{}^2 - (1 - M^2)k_{m,n}^2 > 0$$

i.e.,

$$k_{m,n} < \frac{k'_0}{\sqrt{1 - M^2}} \quad (9)$$

otherwise it is cut-off and decays exponentially along the z-direction. In the present work, all cut-on modes are computed in addition to a few amount of cut-off.

The term $N_{m,n}^2$ in Eq. 5 is a mode normalization that should satisfy the energy conservation over the surface \mathbf{S} , in this case, a circumference with radius a

$$S^{-1} \int_{\mathbf{S}} |\varphi(\vec{r})|^2 d\mathbf{S} = 1 \quad (10)$$

Solving that we have

$$N_{m,n}^2 = \left(1 - \frac{m^2}{(k_{m,n}a)^2}\right) |J_m(k_{m,n}a)|^2 \quad (11)$$

The present formulation allows us to compute the steering vector in the rotating reference frame. Remembering the Eq. 1 for the beamforming imaging, the cross-spectral matrix (CSM) must be also computed in the rotating frame. Two techniques for that are exposed in the next section.

3 SIGNAL PROCESSING TECHNIQUES

3.1 Time domain: Linear interpolation

The principle behind this technique proposed by Herold [5] consists of creating virtual microphone measurements (that physically do not exist) from static pressure measurements recorded in the circular array. If we fix a rotating point with same speed and direction as the fan, the interpolated sound pressure at this point in a certain time will be the average of the neighboring microphones in the wall-mounted array, weighted by its angular spacing from that point to the microphones, just as a linear interpolation.

Mathematically speaking, let N_c be the number of equally spaced microphones on a ring and $p_m(t)$ be the measured sound pressure in the m -th microphone ($m = 1, \dots, N_c$). The angle α between each microphone is given by $\alpha = 2\pi/N_c$.

If we define the time-dependent angle of the measured point $\varphi(t)$ by the angle position from some reference point in the rotating frame at speed Ω , the limit index, lower and upper (m_l and m_u respectively) of the static microphone signals in which we can interpolate is calculated by

$$m_l(m, t) = \left\lfloor m + \frac{\varphi(t)}{\alpha} - 1 \right\rfloor \bmod N_c + 1 \quad (12a)$$

$$m_u(m, t) = \left\lfloor m + \frac{\varphi(t)}{\alpha} \right\rfloor \bmod N_c + 1 \quad (12b)$$

where $\lfloor \cdot \rfloor$ denotes the floor function and “mod” is the congruence operator. Thus, the weighting factors for the respective sound pressures are given by

$$s_u(t) = \frac{\varphi(t)}{\alpha} - \left\lfloor \frac{\varphi(t)}{\alpha} \right\rfloor \quad (13a)$$

$$s_l(t) = 1 - s_u(t) \quad (13b)$$

Finally, the interpolated microphone signals $p_{\Omega, m}$ in the rotating frame is calculated by

$$p_{\Omega, m}(t) = s_l p_{m_l} + s_u p_{m_u} \quad (14)$$

Once calculated, the virtual rotating signal $p_{\Omega, m}(t)$ is then synchronized with same speed with respect to the fan about an axis of interest. The CSM for the virtual rotating array is then estimated equivalently to the stationary case from the $p_{\Omega, m}(t)$ signals.

3.2 Frequency domain: Motion compensation

As far as we know, the first approach for virtual rotating technique based on compensation in frequency domain was proposed by Lowis on [7]. Recently Pannert published [9] experimental results for a rotating source in free-field using the same approach.

Once the array data are in frequency domain, the technique consists of applying spatial Fourier transformation to one ring to obtain data in the “modes domain”. Once in this space, each equivalent mode order “ m ” is frequency-shifted to compensate for the motion effect of the sound source. After that, inverse spatial Fourier transform is applied and data are already motion compensated.

Lewis and Pannert demonstrated that this has same effect as if the microphones were rotating around the duct axis at same speed as the fan.

Mathematically, owing to the sound periodicity in the θ direction, the measured pressure in a ring of equally spaced microphones can be written as a discrete Fourier series as

$$p_m(z, a, \omega) = \frac{1}{N_c} \sum_{i=1}^{N_c} p(z, a, \theta_i, \omega) e^{-jm\theta_i} \quad \left(\frac{-|1-N_c|}{2} \leq m \leq \frac{N_c}{2} \right) \quad (15)$$

where θ_i and z are the i^{th} microphone azimuthal position and distance to a reference plane, respectively. a is the duct radius and p_m is the pressure amplitude of the m^{th} spinning mode.

Once in “modes domain”, the sound pressure of the virtually rotating microphones is obtained by the inverse spatial Fourier transform of the frequency shifted spinning modes $p_m(z, a, \omega + m\Omega)$ as

$$p_\Omega(z, a, \theta_i, \omega) = \sum_{m=-m-}^{m+} p_m(z, a, \omega + m\Omega) e^{+jm\theta_i} \quad (16)$$

where $m+$ and $m-$ are same as in Eq. 15, Ω is the shaft speed and p_Ω is already the sound pressure for the i^{th} microphone in the rotating reference frame and in frequency domain. The term $\omega + m\Omega$ selects different frequencies terms in p_m depending on the spinning mode order and shaft speed for the inverse spatial Fourier transform. This technique is roughly similar to a modulation process [10].

4 RESULTS

The acoustic pressure data from the array and encoder signal were simultaneously acquired at 51.2 kHz sample rate with no shaft-synchronizing system. This was followed by removal of strong fan tones (from 1st to 5th BPF order) from the broadband noise through a time domain algorithm to estimate and subtract the corresponding sinusoids from the raw signal. Subsequently, data was time-resampled to an equivalent 512 samples per fan revolution.

Both techniques were used to perform the virtual rotating microphones, followed by estimation of the cross spectral matrix using Welch’s method, 50% overlapping, Hanning data window of 2048 samples [10]. The well-known technique of CSM main diagonal removal [8] was used to avoid boundary and shear layer noise from the signals.

Conventional rotating beamforming was subsequently performed. Due to the distance from the array to the fan stage, (± 0.86 m for the closest ring), all cut-on modes are analysed plus only a few number of cut-off. Deconvolution method Clean-SC [11] was subsequently applied.

Beamforming maps are in decibels (dB) referred to the sound pressure of $20 \mu\text{Pa}$. x-axis and y-axis are labeled in meters. At the top of each map the frequency for the evaluation is displayed, along with the Mach flow speed, rotating beamforming beam speed and focal plane distance. Each plot is compared side-by-side for the same frequency for both techniques. Power spectral density (PSD) was obtained by the average of all 77 microphones in the array and displayed also in decibels (dB) referred to $20 \mu\text{Pa}$.

In Fig. 3 we see the 1st to 5th BPF tone free static spectra (black curve). Equivalent BPF for 4250 RPM are marked in the x-axis. It is possible to notice that both technique for VRM led to a very similar shape spectra. Above 1.5 BPF there is a constant difference in the PSD level.

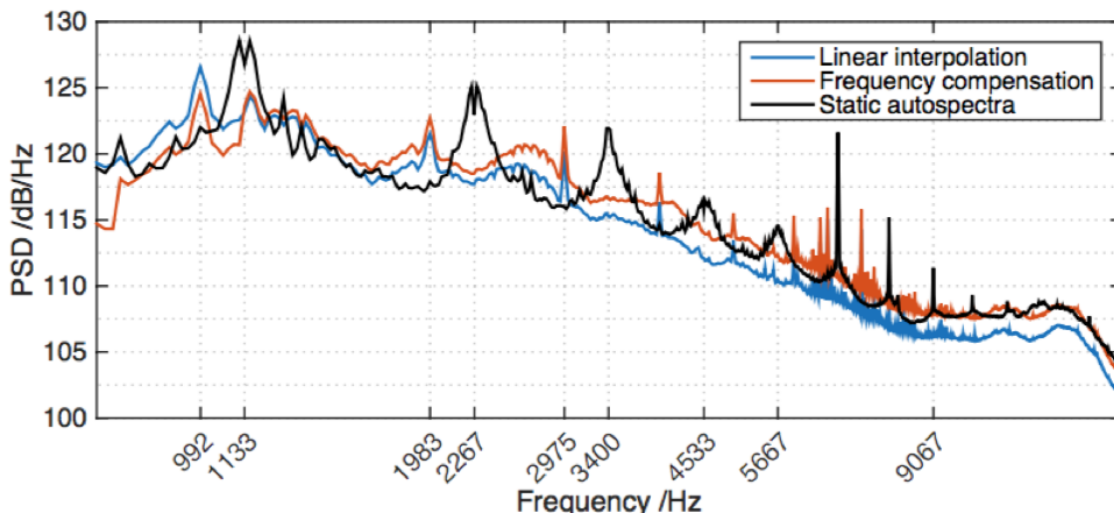


Figure 3: Averaged power spectral density (PSD) for: Time domain linear interpolation (**blue**) and Frequency domain motion compensation (**orange**). Tone free static PSD is also shown in black. Fan at 4250 RPM and 0.1 Mach flow. 1st to 5th and 8th BPF sticks are marked. Sound pressure referred to 20 μ Pa.

Note that all tone peaks appear in both spectras. For frequencies bellow 1.5 BPF the linear interpolation technique has more power than the frequency compensation.

Tone peaks are seen in the rotating PSD for frequencies just bellow the BPF for the static PSD. We believe that their frequency respect to BPF shifted to the rotating frame, just as introduced by Eq. 8. It is known that modes at BPF are Tyler-Sofrin modes [13], i.e., for a fan with 16 blades and 14 stator vanes, the mode $m = +2$ is produced for the first BPF, $m = +4$ for the second and so on. The Tyler-Sofrin mode analysis for that same fan rig was already performed in [2]. In this way, the first BPF tone will appear in the rotating frame with the frequency

$$f_1' = 1133 - 2 \times 4250/60 = 991.7$$

and for the second BPF

$$f_2' = 2267 - 4 \times 4250/60 = 1983$$

both marked on the plot.

Results for conventional rotating beamforming are portrayed in Figs. 4 and 5. On Fig. 4 top plots we see a great difference in the estimation of the noise location. Frequency compensation method was able to detect much more blade-tip noise than the linear interpolation. Same result is observed in mid and bottom plots. A clear pattern of 16 noise sources is seen in right plots, corresponding to the 16 blades in the rotor fan. Furthermore, smeared noise coming from the blade's root is also observed.

For this range of frequencies, $f < 3 \text{ kHz}$, the frequency compensation method showed a much better resolution, i.e., the different noise sources are clearly distinguishable whereas linear interpolation results led only to smeared noise.

Fig. 5 top plots ($f = 3.45 \text{ kHz}$) show a quite similar results. Smeared noise coming from the blade's root and some noise coming from the mid of the blades. Mid plots the 16 noise source

pattern is seen again and quite different results are seen for both techniques. Bottom plots show blade's root noise for interpolation technique whereas frequency compensation does not. The 33 noise source pattern observed in the wall is not noise produced by the fan, but artifacts due to the beamforming technique (as the array has one ring with 33 mics).

Finally, results for Clean-SC deconvolution are displayed in Fig. 6. Those results are even more different for each technique. Blade tip noise can be seen in top-right plot. Mid plots ($f = 2.46 \text{ kHz}$) and bottom plots ($f = 3.81 \text{ kHz}$) are same frequencies evaluated with conventional beamforming in Figs. 4 and 5.

5 CONCLUSIONS

The different techniques implemented here were tested with experimental data from a fan rig constructed at University of São Paulo - Brazil. Results observed are consistent for both techniques.

PSD for both techniques were quite similar in terms of shape and correspondent tones observed. For frequencies below the first BPF linear interpolation technique got about 2 dB higher. However, from 1.5 BPF to higher frequencies the frequency compensation remained approx. 2 dB higher in comparison to the linear interpolation.

Tones were observed in the rotating PSD for both techniques in the exact same frequency. We believe that they are BPF tones in the rotating frame, shifted in frequency respecting their associated mode and fan shaft speed.

In terms of beamforming imaging, the frequency compensation technique showed a better spatial resolution leading to a greater capability to distinguish close noise sources. On the other hand, the linear interpolation method showed maps with noise commonly coming from the inner space and we could not detect tip-noise with this technique. Smeared noise was observed in most of results.

Clean-SC did not perform well with modal steering vectors in most of the cases in our experiment. For a few frequencies tip noise was clearly detected by this deconvolution technique. However, the major maps, for conventional beamforming, the clearly seen pattern of 16 noise sources led to a deconvoluted map with no pattern of distributed sources. The possible reasons for this bad performance of Clean-SC would be: not enough number of microphones in the array; inaccurate formulation for the steering vector; array not close enough to the fan rotor.

ACKNOWLEDGMENTS

The USP fan rig test facility was financially supported by FINEP (Federal funding for development of science and research) and was designed & assembled by technicians and engineers of USP-São Carlos and Escola Politécnica Engineering Schools with the cooperation from EM-BRAER's engineering team, inside the *AERONAVE SILENCIOSA* Project. The authors thank all involved in this project, including NASA Glenn Research Center staff, specially Daniel Sutliff, whose support and technical insight proved very helpful.

References

- [1] C. L. Beattie. “Table of first 700 zeros of Bessel functions - $J_l(x)$ and $J'_l(x)$.” *Bell System Technical Journal*, 37(3), 689–697, 1958. doi:10.1002/j.1538-7305.1958.tb03881.x.
- [2] L. C. Caldas, R. G. Cuenca, R. Q. Lauterjung, and L. A. Baccala. “In-duct beamforming noise source estimation and mode detection at the university of são paulo fan rig.” In *21st AIAA/CEAS Aeroacoustics Conference*. American Institute of Aeronautics and Astronautics, 2015. doi:10.2514/6.2015-2233. URL <http://dx.doi.org/10.2514/6.2015-2233>.
- [3] R. P. Dougherty and B. E. Walker. “Virtual rotating microphone imaging of broadband fan noise.” In *15th AIAA/CEAS Aeroacoustics Conference (30th AIAA Aeroacoustics Conference)*. American Institute of Aeronautics and Astronautics, 2009. doi:10.2514/6.2009-3121. URL <http://dx.doi.org/10.2514/6.2009-3121>.
- [4] L. Enghardt, A. Moreau, and P. Kausche. “Active control of fan tones by means of trailing edge blowing.” In *21st AIAA/CEAS Aeroacoustics Conference*. American Institute of Aeronautics and Astronautics, 2015. doi:10.2514/6.2015-2828. URL <http://dx.doi.org/10.2514/6.2015-2828>.
- [5] G. Herold and E. Sarradj. “Microphone array method for the characterization of rotating sound sources in axial fans.” *Noise Control Engineering Journal*, 63(6), 546–551, 2015.
- [6] R. A. Loew, J. T. Lauer, J. McAllister, and D. L. Sutliff. “The advanced noise control fan.” *NASA/TM-2006-214368, also AIAA-2006-3150*, 2006.
- [7] C. R. Lowis. *In-duct measurement techniques for the characterisation of broadband aero-engine noise*. Ph.D. thesis, University of Southampton, Southampton, England, 2007.
- [8] T. J. Mueller. *Aeroacoustic Measurements*. Springer, 2001.
- [9] W. Pannert and C. Maier. “Rotating beamforming - motion-compensation in the frequency domain and application of high-resolution beamforming.” *Journal of Sound and Vibration*, 333(7), 1899–1912, 2014.
- [10] D. B. Percival and A. T. Walden. *Spectral Analysis for Physical Applications*. Cambridge University Press, 1993.
- [11] P. Sijtsma. “Clean based on spatial source coherence.” In *13th AIAA/CEAS Aeroacoustics Conference (28th AIAA Aeroacoustics Conference)*. AIAA, 2007.
- [12] P. Sijtsma. “Feasibility of in-duct beamforming.” In *13th AIAA/CEAS Aeroacoustics Conference (28th AIAA Aeroacoustics Conference)*. American Institute of Aeronautics and Astronautics, 2007. doi:10.2514/6.2007-3696.
- [13] J. M. Tyler and T. G. Sofrin. “Axial flow compressor noise studies.” *Transactions of the society of automotive engineers*, 70, 309–32, 1962. doi:10.4271/620532.

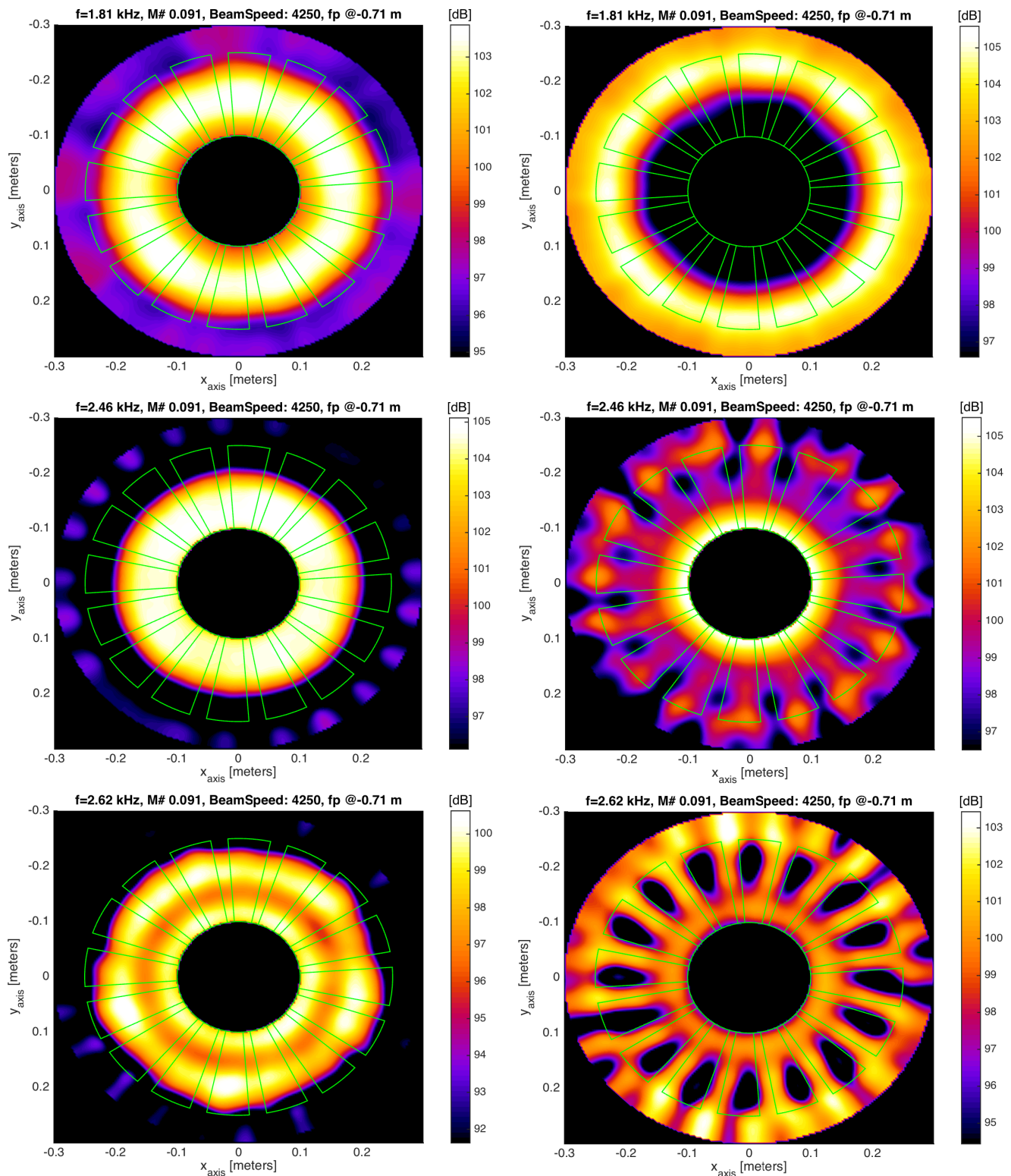


Figure 4: Rotating conventional beamforming. Fan at 4250 RPM and Mach flow 0.1. Focal plane at the fan distance. **Left side:** Time domain linear interpolation. **Right side:** Frequency domain motion compensation.

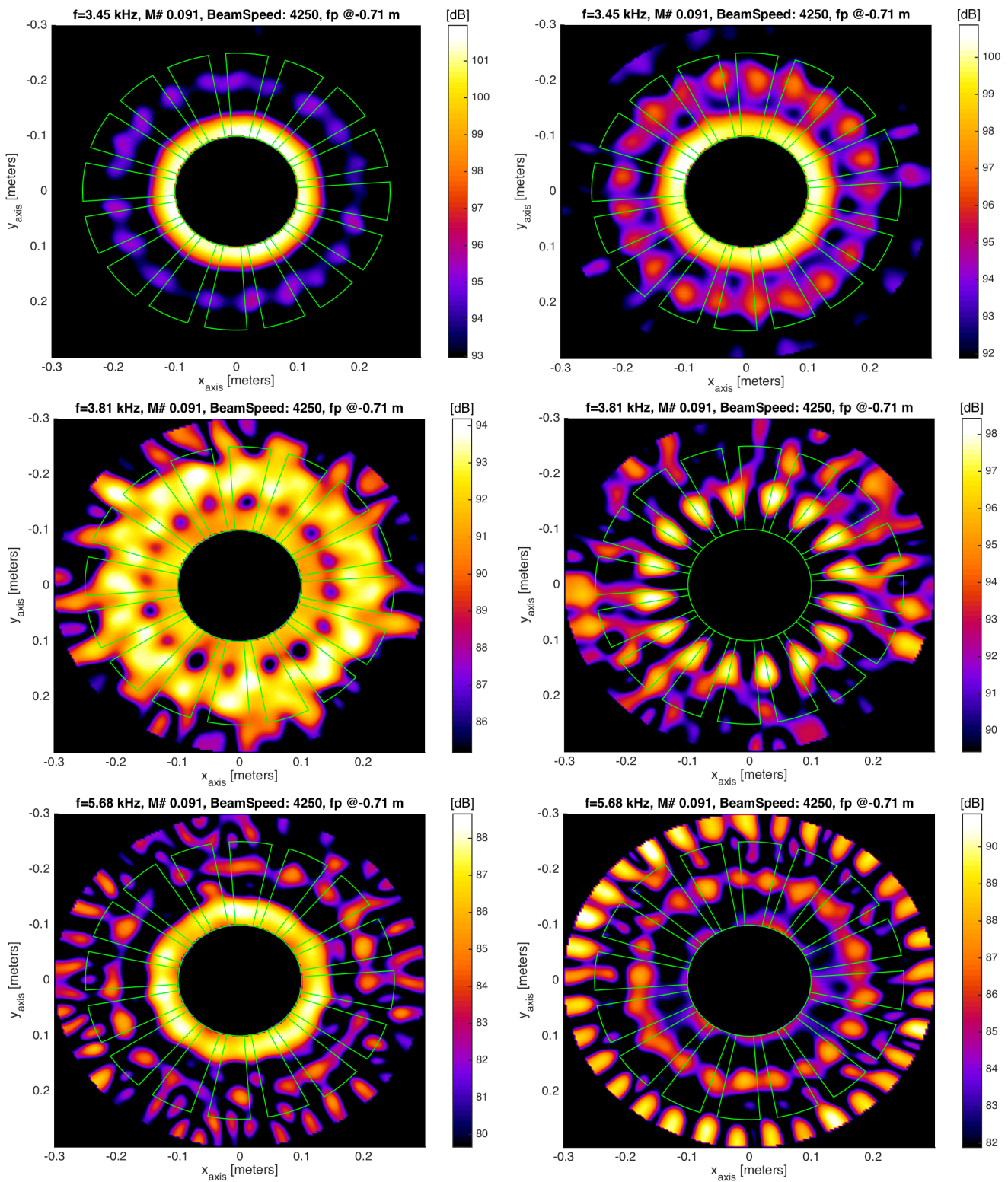


Figure 5: Rotating conventional beamforming. Fan at 4250 RPM and Mach flow 0.1. Focal plane at the fan distance. **Left side:** Time domain linear interpolation. **Right side:** Frequency domain motion compensation.

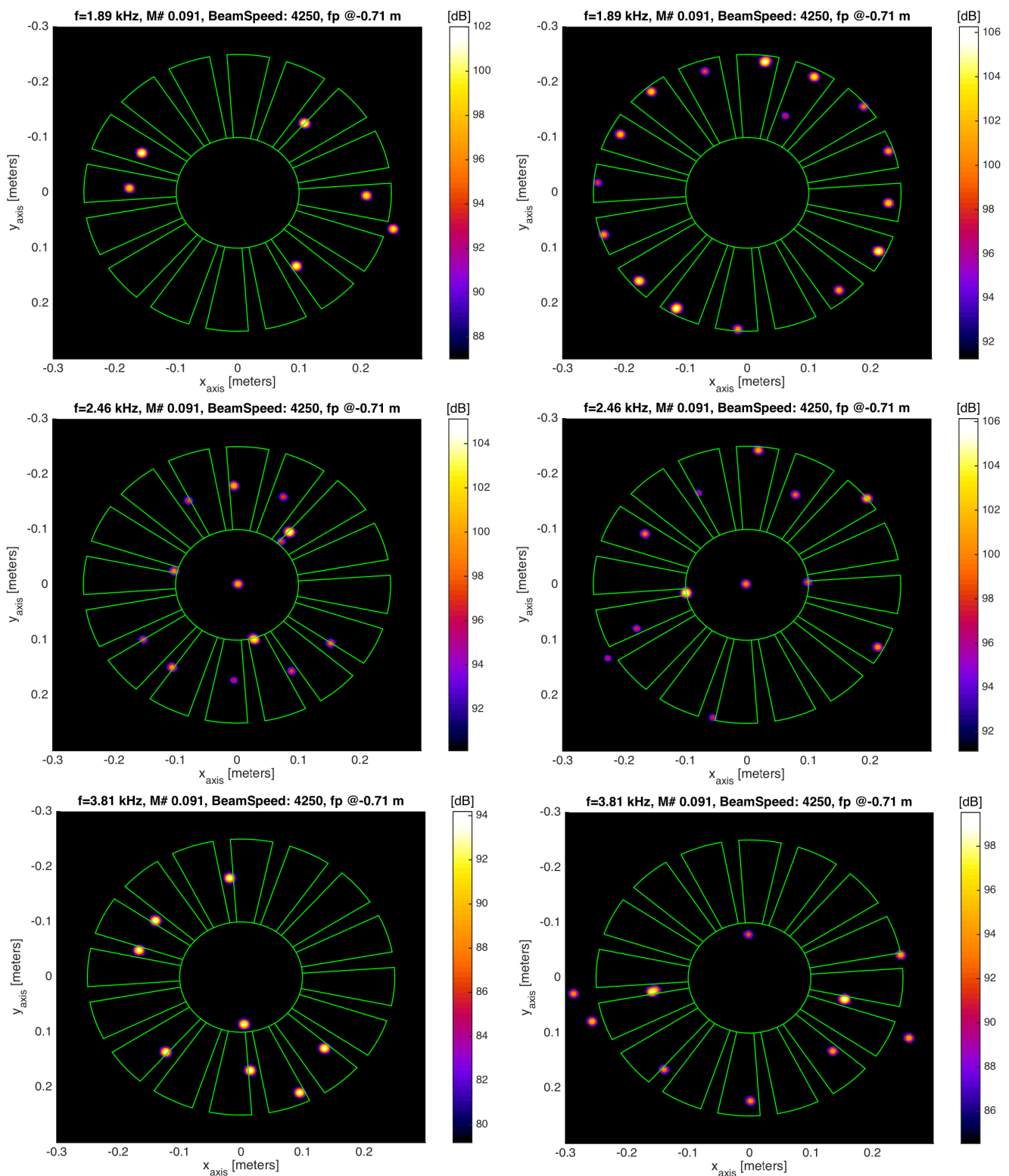


Figure 6: Rotating conventional beamforming with Clean-SC deconvolution. Fan at 4250 RPM and Mach flow 0.1. Focal plane at the fan distance. **Left side:** Time domain linear interpolation. **Right side:** Frequency domain motion compensation.